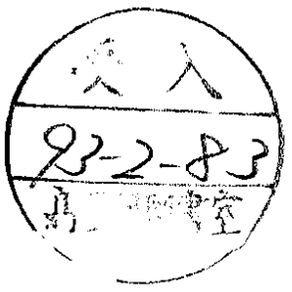

EUROPEAN ORGANIZATION FOR NUCLEAR RESEARCH

CERN-PPE/92-181
30 September 1992

A Microstrip Decay Detector for Beauty Physics

M. Adinolfi[4], C. Angelini[4], D. Barney[3], A. Cardini[4], B.R. French[1], R.B. Hurst[2], C. Lazzeroni[4], P. Martinengo[2], A. Menetrey[1], C. Roda[4], L. Rossi[2]

1 CERN, European Organization for Nuclear Research, Geneva, Switzerland.
2 Dipartimento di Fisica and INFN, Genova, Italy.
3 Imperial College, London, United Kingdom.
4 Dipartimento di Fisica and INFN, Pisa, Italy.

Abstract

The Decay Detector is a compact array of 10 μm pitch silicon microstrip detectors designed to give charged track data which is sufficient, both in quantity and in precision, to allow reconstruction of beauty particle decays. It has been built for Beatrice, a fixed-target hadroproduction experiment at CERN. This "electronic bubble chamber" consists of sixteen 5 mm $\times$ 5 mm microstrip planes comprising more than 8000 detector channels packed into a volume of less than 0.8 cm^3. The pulse heights of all channels are read by analogue front-end electronics and are then compared with individually set thresholds and pedestals. The performance of the Decay Detector has been studied in a test beam and data are presented on its spatial precision, efficiency, and other characteristics.

(Submitted to Nuclear Instruments and Methods in Physics Research)

Fixed target experiments have an important advantage over colliding beam experiments for studying beauty physics. The beauty particles are produced with a large forward boost and decay in a region which can be equipped with detectors, rather than being produced inside a beam pipe where event reconstruction involves extrapolation from remote measurements. However, attempts to study beauty physics with fixed target experiments have so far had limited success. Although thousands of beauty events must have been produced in fixed target experiments, few have been reconstructed. The main drawback of fixed target experiments lies in the small beauty production cross section, $\sim 10^{-6}\,\sigma_{tot}$ for hadroproduction. An efficient means for extracting the signal from this large background is crucial. One approach is based on identification of the sequential decay topology of a beauty particle followed by a charm particle. However these events, with multiple decay vertices and high track densities, challenge the capabilities of conventional vertex detectors. The two fixed target experiments which have succeeded in reconstructing and identifying beauty decays have used emulsion stacks to obtain the required track resolution of a few microns [1,2]. With this technique it is practical to collect a data sample containing, at most, a few tens of reconstructed beauty events. Silicon microstrip detectors offer the advantage of fast response time and electronic readout and should allow a higher rate, higher statistics experiment to be performed. Beatrice (also known by the CERN code WA92) is designed to be such an experiment. An array of 10 μm pitch microstrip detectors, collectively known as the Decay Detector, has been built to instrument the beauty decay region, the first few centimeters downstream of the target. This paper describes the mechanical and electronic structure of the Decay Detector and gives results on its performance in a test beam.

Structure of the Decay Detector

The Decay Detector has been designed to allow detailed reconstruction of B decays which occur within its volume. It consists of sixteen 10 μm pitch silicon microstrip planes placed within 3.2 cm of the target (see Fig. 1). The first microstrip detector is 1.2 mm downstream of the target, about 1/4 of the average decay length of beauty particles produced by the 350 GeV π^- beam used by WA92. This detector is followed by 12 additional microstrip planes spaced 1.2 mm apart, all with the same orientation, to allow precise track reconstruction in one projection. The array is completed by three microstrip planes with different orientations which aid in linking the projected tracks found in the decay detector with space tracks reconstructed in downstream detectors. Each of the sixteen microstrip planes has 512 channels covering a 5 mm $\times$ 5 mm surface, thus there are 8192 channels packed into a volume of less than 0.8 cm^3.

The microstrip detectors used were manufactured by Micron Semiconductor Ltd[1] in two thicknesses, 300 μm and 150 μm. To minimize secondary interactions and multiple scattering in the region closest to the target 150 μm thick detectors, each corresponding to 3.3×10^{-4} interaction lengths and 1.6×10^{-3} radiation lengths, are used for the first six microstrip planes. The 300 μm thick detectors are used for the remaining 10 planes due to their higher detection efficiency. A microstrip detector with 10 μm pitch was first

[1]Lancing, Sussex, U.K.

used in an experiment by the WA82 collaboration. The satisfactory performance of that device led to the decision to use similar detectors in the current experiment. Some details of the WA82 microstrip construction which are also relevant to those used here may be found in reference [3].

Although the active area of the microstrip detectors is 5 mm × 5 mm, they are fabricated on 14 mm × 14 mm silicon chips, the extra surface being used for fanouts. Alternate channels are fanned out to opposite sides of the chip and further separation of neighboring channels is achieved by having two rows of bonding pads on each side of the chip so that a bonding pitch of 80 μm is obtained. Each chip is mounted in a 14.2 mm square hole cut in the center of a 250 μm thick, 46 mm × 46 mm piece of Al_2O_3 ceramic. The ceramic serves as both a mechanical support and as a second stage fanout (see Fig. 2). The bonding pads on the microstrips are connected by ultrasonically bonded 25 μm aluminum wires to gold tracks laid down on the surface of the ceramic. The gold tracks terminate on the four outer edges of the ceramic, 128 channels on each side, at a pitch of 250 μm. Kapton foils with overlaid gold tracks are glued to the edges of the ceramic and electrically connected by 25 μm aluminum wires, again by ultrasonic bonding. These kapton foils serve as the third stage of fanout (see Fig. 3). At their outer edges pin connectors at a pitch of 1.27 mm plug into printed circuit cards containing the front-end electronics.

The required mechanical stability of the detector array is obtained by the following support system. The ceramic fanout pieces in which the microstrips are mounted are held at their corners in a 10 cm × 10 cm × 4 cm box made of the same ceramic material (Al_2O_3) so that incompatibilities due to thermal expansion and contraction are avoided. This box is intended to maintain the microstrips in stable positions relative to each other. The detectors are mounted inside it to tolerances of 1 mrad in angle about the beam axis and 10 μm longitudinally. During the course of a 2 day test beam run variations in the relative transverse positions of the microstrips averaged 0.4 μm rms and were 0.6 μm rms in the worst case. The ceramic box is mounted inside a larger box, 24 cm × 24 cm × 8 cm, constructed mostly from fiberglass and brass, which also contains the target and provides a clean environment for the detectors (see Fig. 4). The front and rear windows of the box are 25 μm mylar, aluminized so that the interior is shielded from light and, to a lesser extent, from ambient electronic noise. For the test run it was filled with dry nitrogen at atmospheric pressure. The larger box is designed to be mounted with a precision of $\sim$10 μm transverse to the beam axis on a marble optical bench which also supports some other detectors used in the experiment.

Each microstrip plane in the decay detector is connected via the fan-out structure described above to four printed circuit cards which contain analogue front-end electronics. A circuit card holds 8 daisy-chained Amplex [4] chips with 16 channels per chip. Each microstrip channel is directly connected to a charge amplifier, which is followed on the Amplex chip by a shaping amplifier and a track-and-hold stage. The Amplex circuit uses a continuous feedback and time filtering technique so that the output baseline is largely unaffected by the detector leakage current[2] and the circuit is continuously sensitive to input signals, as needed for asynchronous operation in a fixed target experiment with a long spill cycle. The peaking time of the electronics is 500 ns. When an event trigger

[2]typically a few microamps per detector plane

occurs, an appropriately-timed strobe is sent to the track-and-hold stage which causes the signal amplitude to be stored until a reset is issued.

The charge signals held by the Amplex are read out serially by CAMAC encoding modules called DRAMS (Digital Readout of Analogue Multiplexed Signals) [5]. The DRAMS modules digitize the pulse heights with 8-bit accuracy, compare them to preset thresholds, suppress sub-threshold channels from the data record, and subtract pedestals. Pedestals and thresholds are measured and set individually for each channel in dedicated pulser trigger runs. The thresholds are set to a value $ped + n \cdot \sigma_{ped}$ where ped and σ_{ped} are the mean and width of the measured pedestal distribution for a channel and n is a factor chosen in the range of 3–5. Setting thresholds in this way cancels, to first order, the effect of variations in gain and reduces the number of noisy channels.

Test of the Decay Detector

The performance of the decay detector has been studied with a 50 GeV π^- test beam incident at an angle of ~20 mrad.[3] The array of scintillation counters used for triggering defined a 1 mm square beam spot which was centered on the active area of the microstrips planes. Only the 256 channels in the central region of each detector were read out, so the active area for the test was 2.5 mm × 5 mm. Beam trigger runs of ~1000 events each were taken varying the thresholds over the range 3–5σ and the bias voltages over the range 60–160 V for the 300 μm thick detectors and 30–90 V for the 150 μm detectors. Data were also taken with pulse generator triggers to study the quiescent noise level.

The ionization produced in the silicon by the passage of a particle is frequently collected on more than one channel, therefore analysis of the data began with reconstruction of clusters of adjacent hits. The position of each cluster is taken to be the center of gravity of the hits which compose the cluster, weighted by their pulse heights. The error on the cluster position is $10\,\mu\text{m}/\sqrt{12} \cdot \sqrt{\Sigma p_i^2}/\Sigma p_i$ where p_i is the pulse height of hit i. Tracks are reconstructed by a least squares fit, excluding those clusters $> 20\,\mu$m from the track and requiring that tracks contain clusters in ≥ 5 detector planes and have χ^2 probability ≥ 0.05. Only events with exactly one reconstructed track are used. Results have been obtained on the cluster size and pulse height of signals, signal-to-noise ratio, spatial precision, detection efficiency, and the rate of noise in the detectors.

Typical cluster size distributions for 300 μm and 150 μm detectors are shown in Fig. 5. These distributions are made for a standard set of operating conditions, a bias of 90/45 V (for 300/150 μm planes) and a threshold of 4σ, and only include clusters which are part of a track. The variation of average on-track cluster size as a function of bias voltage and threshold is plotted in Fig. 6. Cluster size is larger for the 300 μm planes than for the 150 μm planes and decreases with increasing threshold. The observed decrease in cluster size with higher bias voltages is due to a smaller lateral spread of the ionization cloud in the silicon because of the shorter collection time. This effect is more evident for the 300 μm thick detectors in which the ionization cloud is more dispersed.

[3] compared with an average dip angle of ~15 mrad for particles produced by 350 GeV interactions in the target

Plane Thickness	Threshold	Efficiency	Multiplicity	Noise
300 μm	3σ	0.99 ± 0.01	1.49 ± 0.02	0.50 ± 0.02
	4σ	0.98 ± 0.01	1.16 ± 0.02	0.17 ± 0.02
	5σ	0.98 ± 0.01	1.09 ± 0.01	0.10 ± 0.01
150 μm	3σ	0.96 ± 0.01	1.40 ± 0.02	0.44 ± 0.02
	4σ	0.91 ± 0.02	1.07 ± 0.02	0.16 ± 0.02
	5σ	0.82 ± 0.02	0.94 ± 0.01	0.13 ± 0.02

Table 1: Efficiency and cluster multiplicity as a function of threshold at $V_{bias} = 90/45$ V. The noise is calculated as the difference between multiplicity and efficiency.

The average pulse height of clusters associated with a track, considering clusters of all sizes, is 44 ADC counts for the 300 μm detectors and 18 ADC counts for the 150 μm planes with the standard 90/45 V bias, 4σ threshold running conditions. The signal-to-noise ratio is calculated as the average pulse height of clusters divided by the width of the pedestal distribution, *i.e.* the same σ_{ped} as used in setting thresholds. For clusters containing more than one channel we assume that the noise contributions of the various channels are independent, thus the mean noise is the quadratic sum of the contributions. With 90/45 V bias and 4σ thresholds S/N $\simeq$ 12 for the 300 μm detectors and 6 for the 150 μm detectors, averaging over all clusters sizes.

The spatial precision of each detector was determined using tracks fit to clusters in all detectors except the one under consideration. The difference distribution between the cluster position predicted by the track and the position of the nearest actual cluster is shown in Fig. 7 for clusters consisting of one hit and two hits. The width of the distribution for single-hit clusters is 3.1 μm, consistent with the expected precision of $10/\sqrt{12}$ μm. Better determination of cluster position with multiple-hit clusters is apparent in the width of the 2-hit cluster distribution, 1.8 μm in this case. These distributions were made using data taken with $V_{bias} = 90/45\,V$ and 4σ thresholds, but the width has little dependence on bias voltage or threshold. The average precision, considering clusters of all sizes, does depend on bias voltage and threshold and, especially, on detector thickness since average cluster size varies with these parameters. Average precision with $V_{bias} = 90/45$ V and 4σ thresholds is 2.0 ± 0.2 μm for the 300 μm thick detectors and 2.9 ± 0.2 μm for the 150 μm thick detectors, where the error represents the spread in the values of precision obtained from the various detectors used.

Efficiencies have been calculated as the fraction of events in which a cluster is present in a microstrip within 10 μm, *i.e.* within about 3–5σ, of the position predicted by a track. As in the measurement of spatial precision, the track parameters were determined from all detectors except the one under consideration. To eliminate acceptance effects, only tracks containing hits in the first and last planes were considered. Efficiency did not change significantly with variations of bias voltage over the voltage range studied; however, it did show appreciable variation with threshold settings, particularly for the 150 μm detectors. Efficiencies obtained at a bias of 90/45 V are shown in Table 1.

Noise in the detectors has been studied with both beam triggers and pulser triggers. For beam trigger events the average number of clusters per plane is shown in Table 1 as a function of threshold; cluster multiplicity showed little variation with changes of

bias voltage. The expected number of clusters in the absence of noise is given by the efficiency; thus subtracting the efficiency from the cluster multiplicity yields an estimate of the noise including such beam correlated noise sources as delta rays, electronic cross talk, and clusters which are split by dead or inefficient channels. We see from Table 1 that the noise is reduced a factor of $\sim$3 in going from 3σ to 4σ thresholds and another factor of $\sim$40% in going to 5σ. With pulser triggers the quiescent noise rate is measured to be $\sim 10^{-1}$ per plane per event with 3σ thresholds, $\sim 10^{-3}$ with 4σ, and less than 10^{-4} (none seen) with 5σ, which are roughly in agreement with a Gaussian distributed noise source scaled by the number of channels per plane. With 3σ thresholds the random noise rate, as measured with pulser triggers, is of the same order of magnitude as the total noise which occurs in coincidence with the beam. With higher thresholds the random noise is insignificant.

In conclusion, the decay detector has been found to function in accordance with our design goals. Spatial precision is $\sim 3\,\mu$m or better, as expected. A threshold of 4σ gives a good compromise between the competing needs of efficiency and noise suppression, both for the $300\,\mu$m detectors and also for the lower signal-to-noise $150\,\mu$m detectors. The decay detector with its "bubble chamber like" tracking capabilities (see Fig. 8) appears to be a device adequate to meet the demands of reconstructing beauty decays produced in hadronic interactions.

It is a pleasure to acknowledge the superb technical work of F. Cossey and R. Pegaitaz in the construction of the decay detector and to thank A. Duane for his important support during data collection, F. Antinori for designing the ceramic fanouts, C. Da Via and L. Lopez for assistance in assembling the detectors, F. Vernocchi for testing the front end electronics, and P. Grafstrom for setting up the beam. The realization of the Decay Detector would not have been possible without the considerable support of E. Chesi, V. Flaminio, E.H.M. Heijne, P. Jarron, and D. Websdale.

References

[1] J.P. Albanese *et al.* (WA75 Collaboration) Phys. Lett.**B158** (1985) 186;

[2] R.A. Sidwell *et al.* (E653 Collaboration) in Proceedings of the 1991 Meeting American Physical Society, Division of Particles and Fields, Vancouver, D. Axen, D. Bryman and M. Comyn eds. (World Scientific,1992) 516.

[3] F.Antinori *et al.* Nucl. Instrum. and Methods **A288** (1990) 82.

[4] E.H.M. Heijne and P. Jarron, "A Low Noise CMOS Integrated Signal Processor for Multielement Particle Detectors", preprint CERN/EF–88–5, April 1988.

[5] E. Chesi and P. Martinengo, "Digital Readout for Analog Multiplexed Signals (DRAMS), CERN experiment PS202 internal note, 11 September 1988.

Figure Captions

Fig. 1 The arrangement of microstrip detector planes along the beam axis. The six planes closest to the target are 150 μm thick; the remaining eight planes are 300 μm thick. Planes 1–13 are oriented to measure positions in the 'Z' direction, vertical in this drawing. Plane 14, labeled 'Y', is rotated 90° about the beam axis relative to the 'Z' planes. Planes 15 and 16, labeled 'U' and 'V', are rotated by 10.14° relative to the 'Z' and 'Y' planes respectively. Note the horizontal and vertical scales in millimeters. The vertical scale of the drawing is 5 times larger than the horizontal scale.

Fig. 2 A 10 μm pitch microstrip detector mounted in its supporting ceramic. The photograph is overlaid with a drawing to make the various regions more distinct. The labeled features are (A) active area of the detector; (B) fanout on the silicon chip; (C) wire bonding between the silicon microstrips and the fanout strips on the ceramic; (D) fanout on the ceramic; (E) wire bonding between the ceramic and kapton foil (bonding is obscured by a protective covering); (F) kapton foil which joins the ceramic to the front end electronics.

Fig. 3 The complete fanout structure for one microstrip plane, including detector, ceramic, and kapton foils. At the outer ends of the kapton foils are pin connectors which attach to the front end electronics (Amplex) printed circuit cards.

Fig. 4 The complete Decay Detector inside the box which is designed to be mounted on an optical bench. A few Amplex cards are installed. The mylar window is removed from the front of the box so that the target mount is visible inside.

Fig. 5 Typical cluster size distribution for (a) 300 μm and (b) 150 μm thick detectors with the standard operating conditions of 4σ thresholds and 90/45 V bias.

Fig. 6 Variation of average cluster size as a function of bias voltage and threshold for the (a) 300 μm and (b) 150 μm thick detectors.

Fig. 7 Difference between measured cluster positions and predicted positions, where the predictions are based on tracks found in the other detectors of the array. The distributions for (a) single-hit cluster and (b) 2-hit clusters have almost identical numbers of entries. Gaussian fits to the distributions are shown by dotted lines and have widths of $\sigma = 3.1\,\mu$m for (a) and $\sigma = 1.8\,\mu$m for (b).

Fig. 8 A 350 GeV π^- interaction as seen by the Decay Detector. Each 'x' represents the reconstructed position of a cluster which may consist of more than one hit. Only the first 13 detector planes (the 'Z' planes) are pictured. All 512 channels are read out.

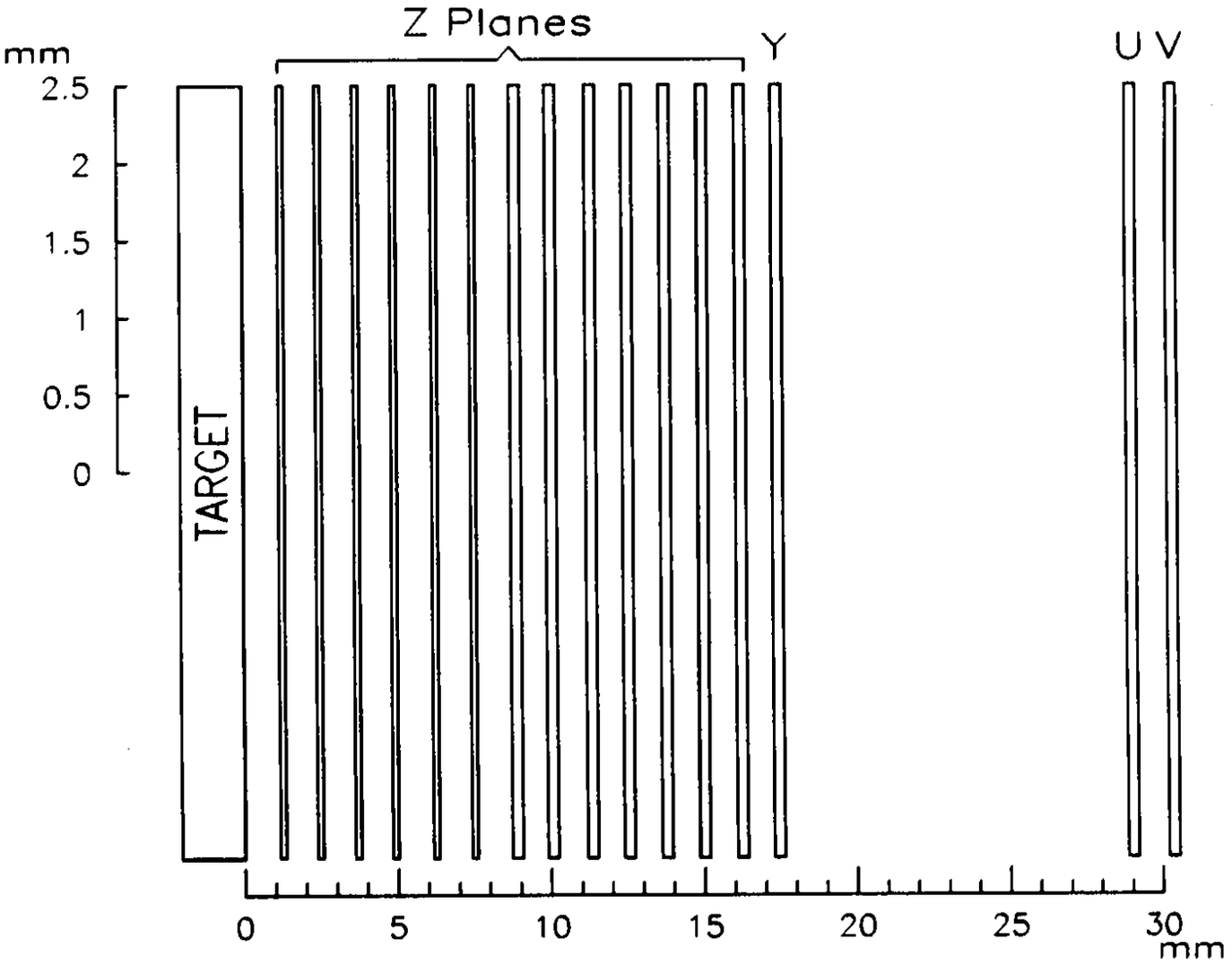

Figure 1

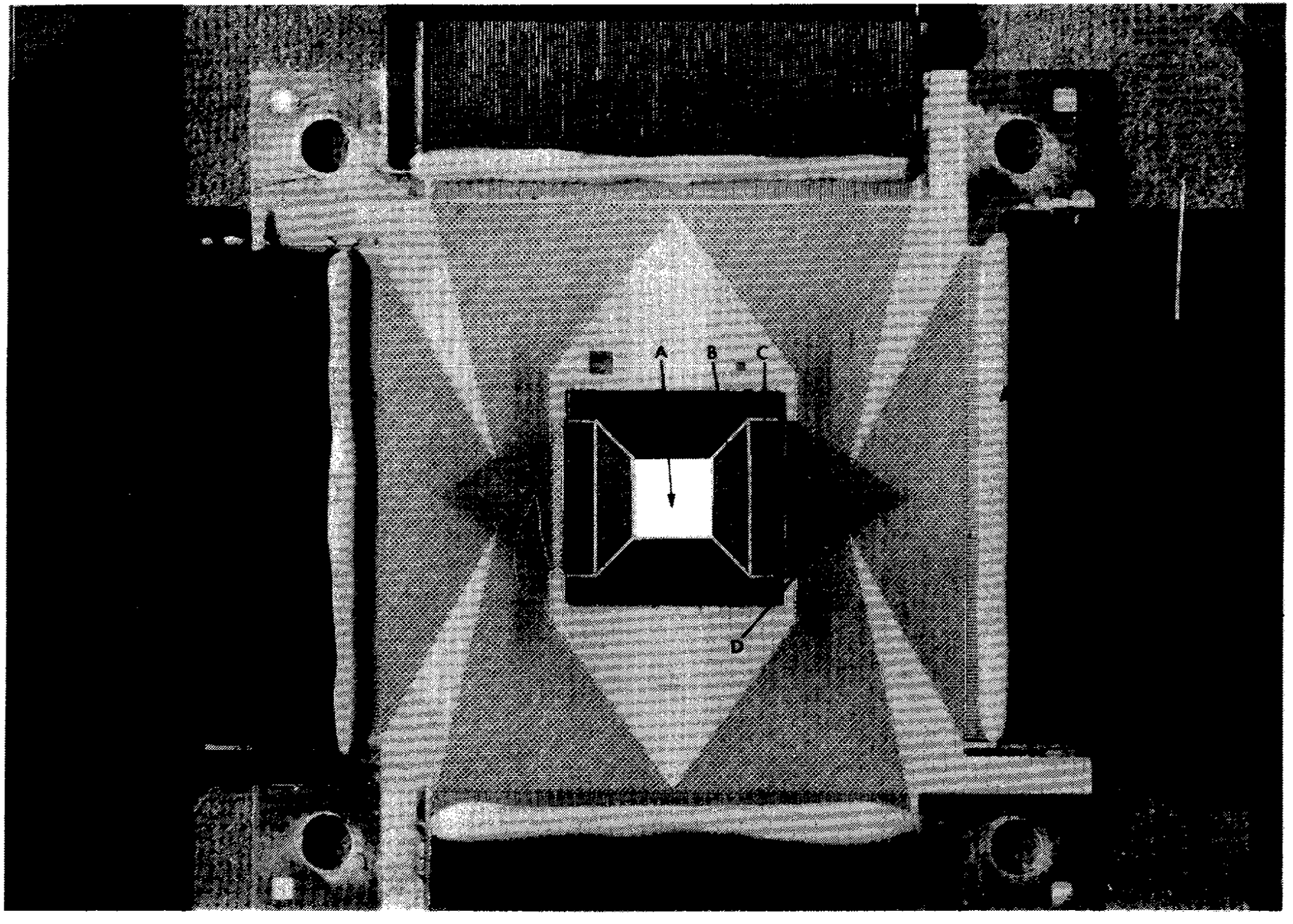

Figure 2

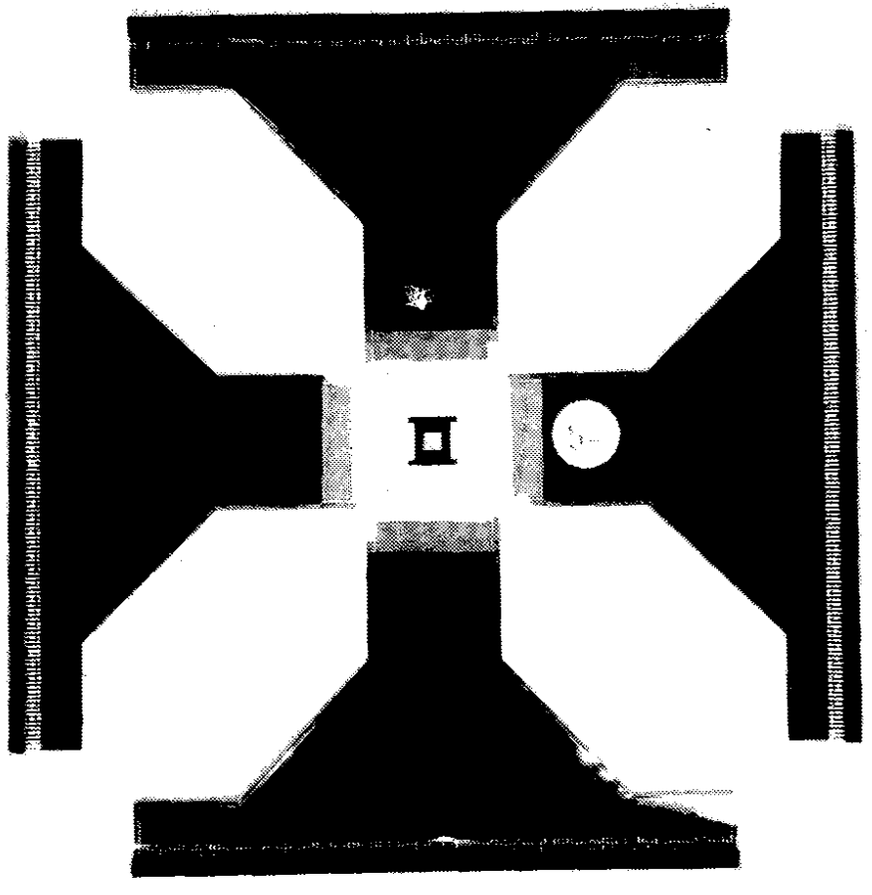

Figure 3

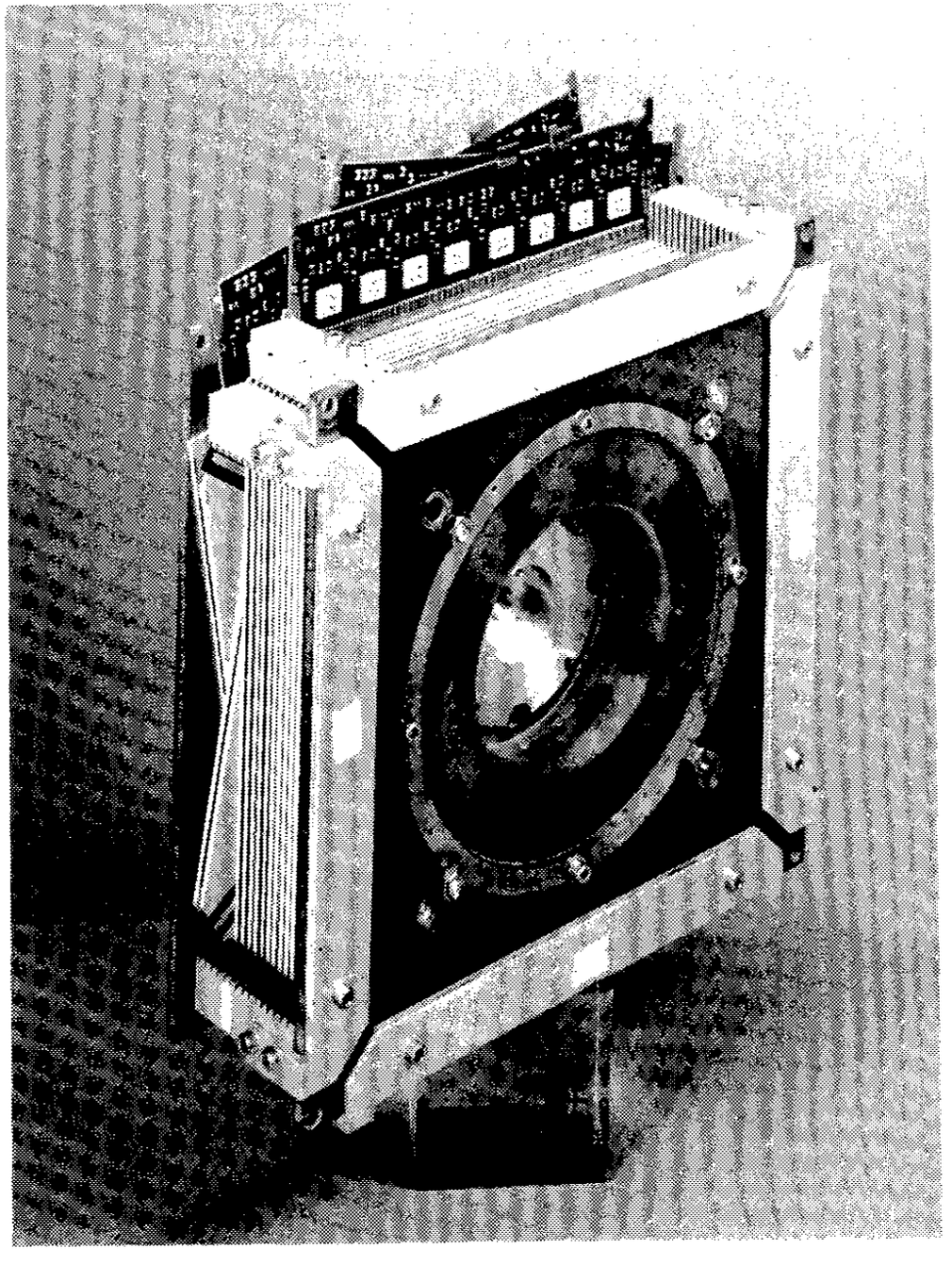

Figure 4

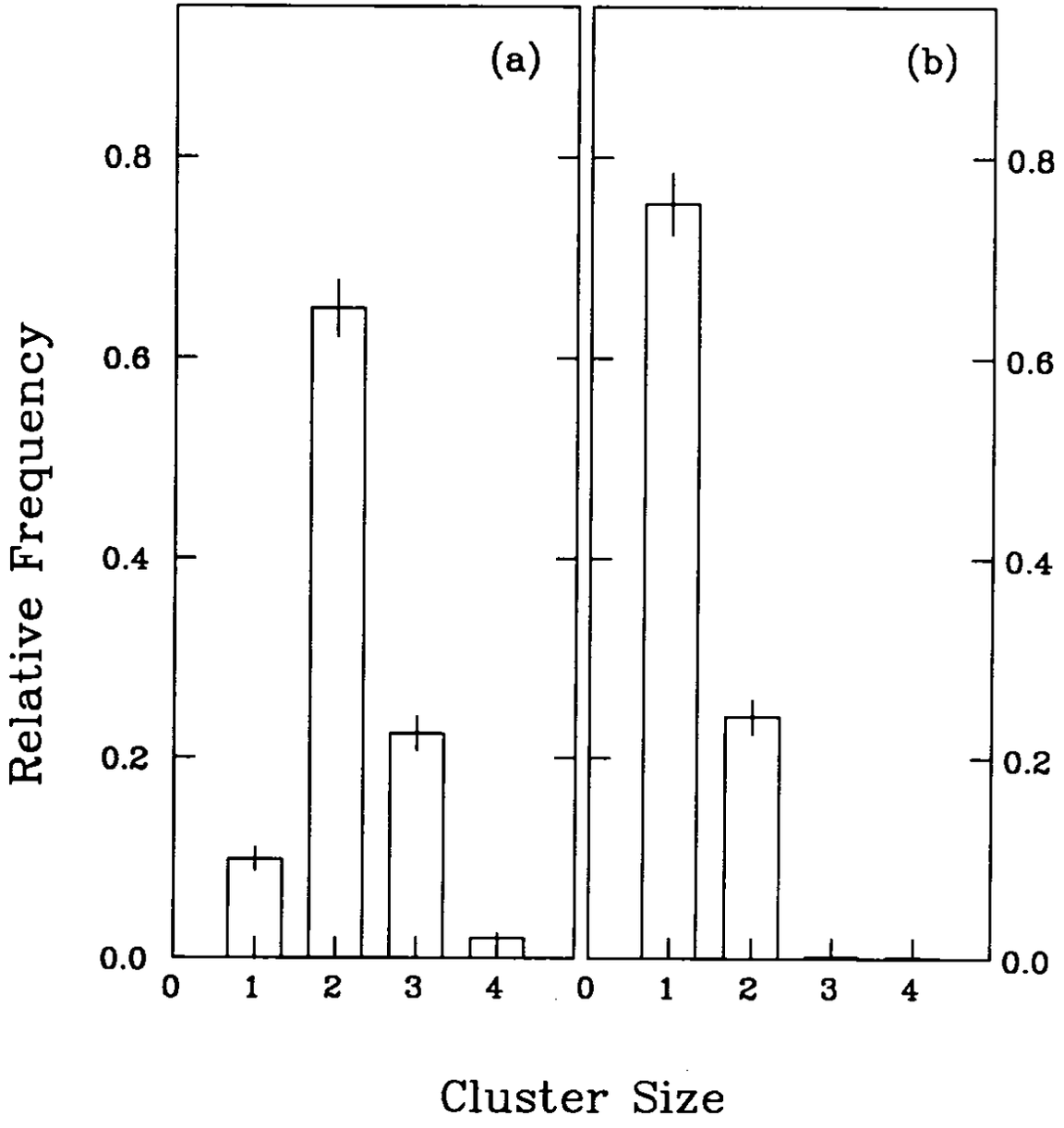

Figure 5

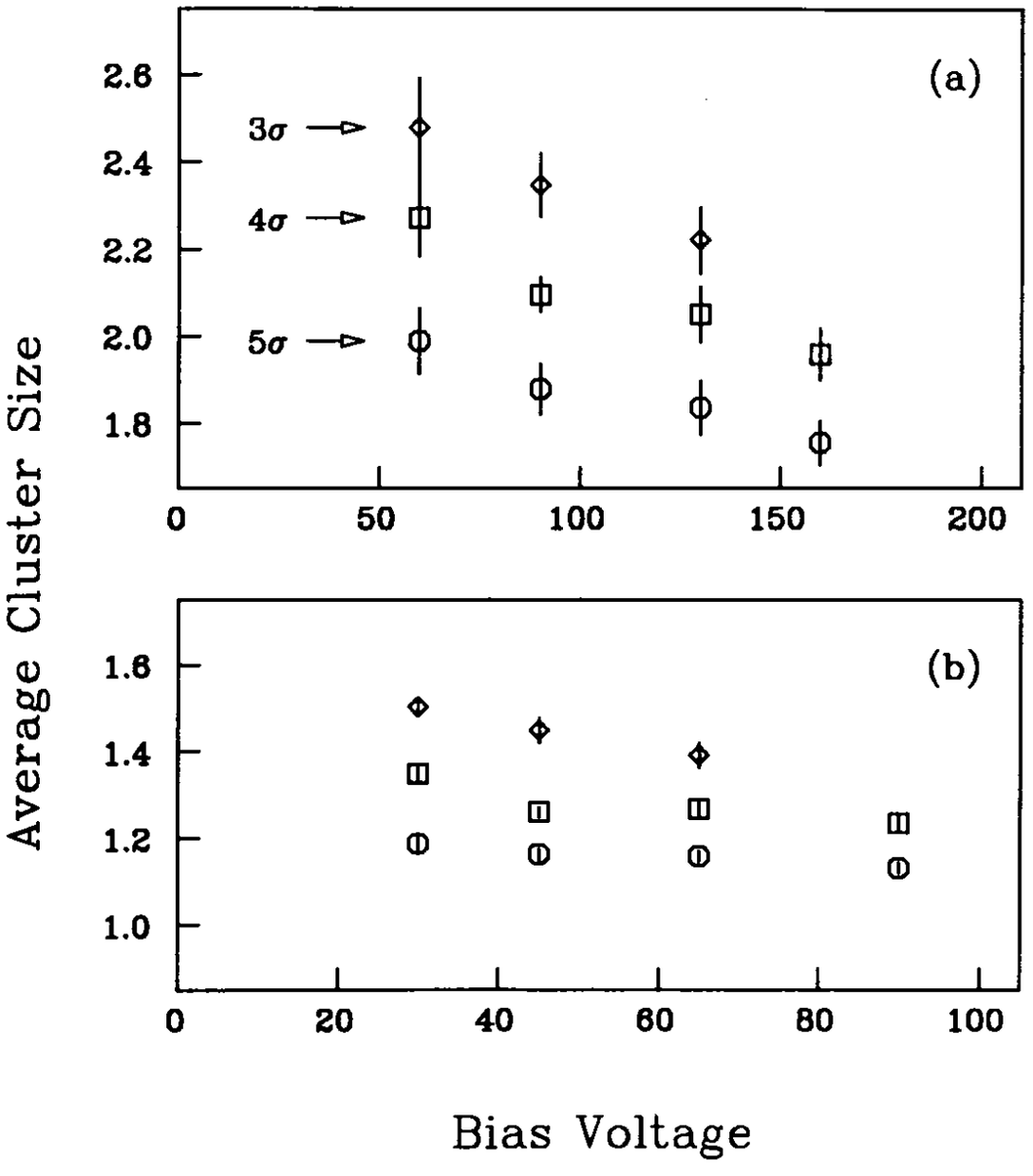
Average Cluster Size
(a)
3σ
4σ
5σ
2.6
2.4
2.2
2.0
1.8
0
50
100
150
200
(b)
1.6
1.4
1.2
1.0
0
20
40
60
80
100
Bias Voltage

Figure 6

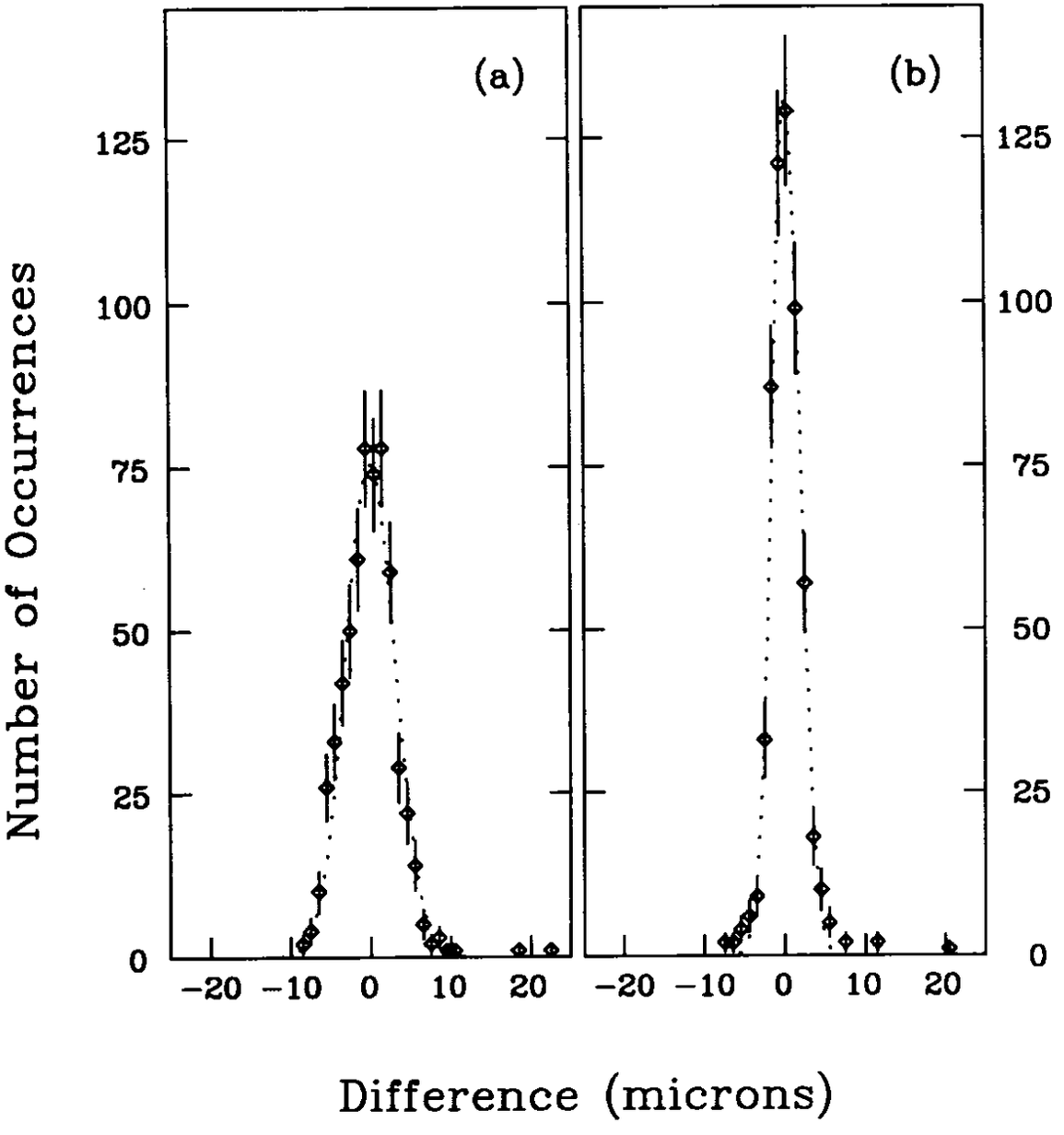
(a)
(b)
125
100
75
50
25
0
−20 −10 0 10 20
Number of Occurrences
Difference (microns)

Figure 7

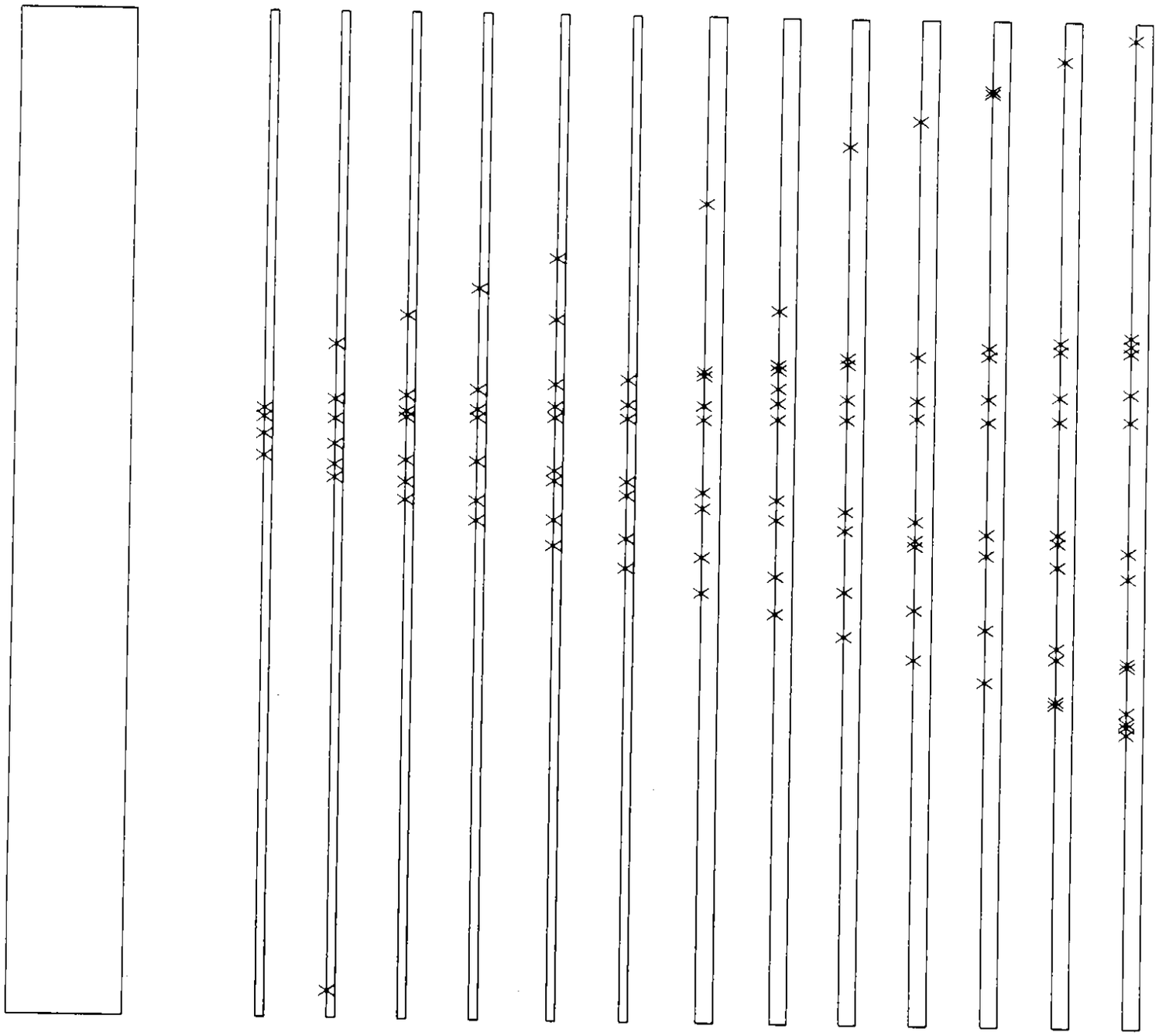

Figure 8